An Implantable Active-Targeting Micelle-in-Nanofiber Device for Efficient and Safe Cancer Therapy

Guang Yang, Jie Wang, Yi Wang, Long Li, Xing Guo, and Shaobing Zhou*

Key Laboratory of Advanced Technologies of Material, Minister of Education, School of Materials Science and Engineering, Southwest Jiaotong University, Chengdu 610031, Sichuan, PR China

ABSTRACT Nanocarriers have attracted broad attention in cancer therapy because of their ability to carry drugs preferentially into cancer tissue, but their application is still limited due to the systemic toxicity and low delivery efficacy of intravenously delivered chemotherapeutics. In this study, we develop a localized drug delivery device with combination of an active-targeting micellar system and implantable polymeric nanofibers. This device is achieved first by the formation of hydrophobic doxorubicin (Dox)-encapsulated active-targeting micelles assembled from a folate-conjugated PCL—PEG copolymer. Then, fabrication of the core—shell polymeric nanofibers is achieved with coaxial electrospinning in which the core region consists of a mixture of poly(vinyl alcohol) and the micelles and the outer shell layer consists of cross-linked gelatin. In contrast to the systematic administration of therapeutics *via* repeatedly intravenous injections of micelles, this implantable device has these capacities of greatly reducing the drug dose, the frequency of administration and side effect of chemotherapeutic agents while maintaining highly therapeutic efficacy against artificial solid tumors. This micelle-based nanofiber device can be developed toward the next generation of nanomedicine for efficient and safe cancer therapy.

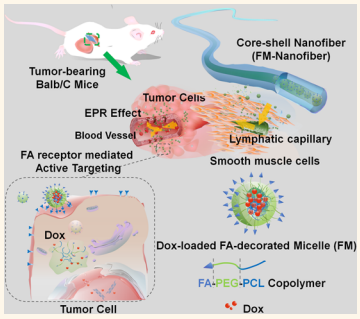

KEYWORDS: localized drug delivery · active targeting · nanocarrier · nanofibers · cancer therapy

Cancer is a major public health problem and remains one of the world's most devastating diseases. Systemic chemotherapy along with surgical resection or radiotherapy is the most commonly used therapeutic strategy for cancer. Some progress has been made in cancer therapy, but there are many limitations including severe toxicity in healthy tissues or even death caused by the systematic administration of anticancer drugs at maximum tolerable doses[1] and the limited distribution of drugs from the blood vessels in solid tumors with chemotherapy,[2] low resection rates and poor overall patient survival in surgery,[3] and serious clinical toxicities in radiotherapy.[4] More recently, to overcome these limitations, nanocarrier-based drug delivery systems have attracted more and more attention.[5−9] These systems have the ability to preferentially carry drugs into cancer tissues or to targeted locations, which is in contrast to systematic administration of free drugs. However, the delivery efficacy of therapeutic agents and in turn the therapeutic effects are still major challenges of these intravenously delivered chemotherapeutics.

Among these nanocarriers, polymeric micelles with distinct core/shell architecture self-assembled from amphiphilic copolymers have been widely reported[10−13] due to their exceptional advantages, such as the ability to improve the solubility of water-insoluble drugs, prolonging blood circulation, and the ease of functionalization.[10,13−16] However, these nanocarriers will encounter numerous barriers en route from the injection site to the target cell, such as mucosal barriers and nonspecific uptake.[17,18] Thus, the intravenously delivered micelles still display some deficiencies, including rapid clearance from the bloodstream with subsequent overaccumulation in nontarget organs,[19,20] overreliance on the EPR effect to deliver the nanocarrier into the tumor, and a modest increase in tumor accumulation.[21] Additionally, the micelles' advantage, prolonging blood circulation, sometimes turns into a problem that may lead to extravasation of the encapsulated cargos in unexpected sites due to the low stability of the micellar system.[7]

To address some of these problems, localized drug delivery to the solid tumors is a

* Address correspondence to shaobingzhou@swjtu.cn, shaobingzhou@hotmail.com.

Received for review August 15, 2014 and accepted January 20, 2015.

Published online January 20, 2015
10.1021/nn504573u

© 2015 American Chemical Society

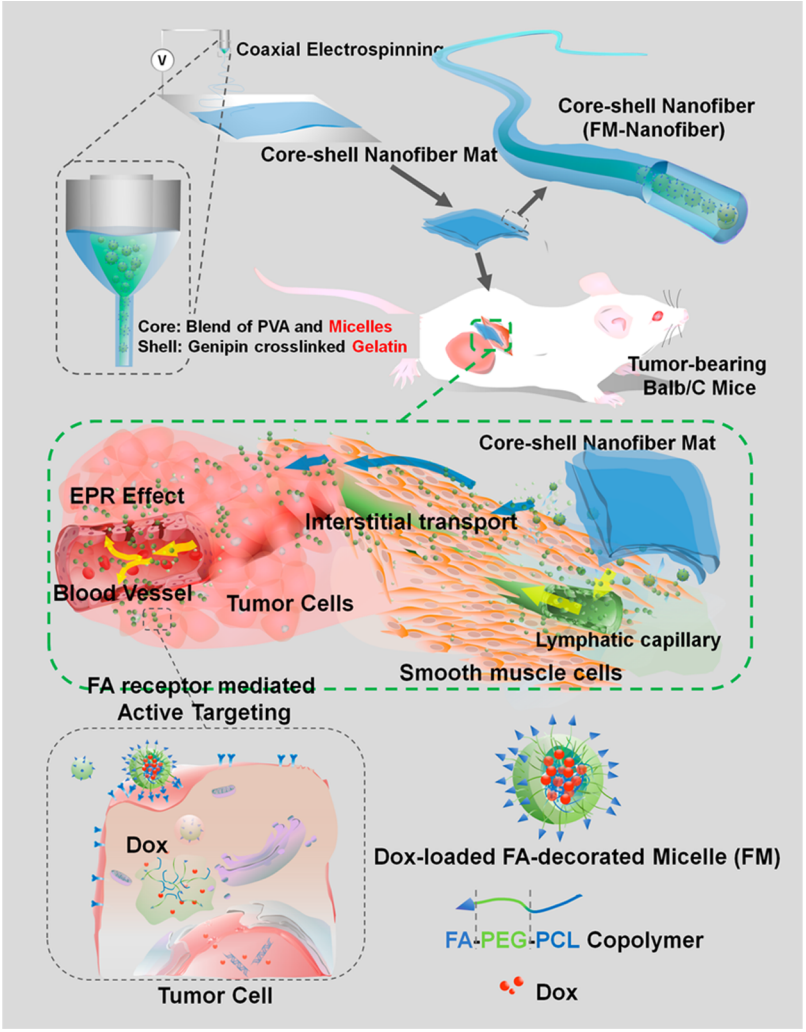

Scheme 1. Schematic illustrations of the fabrication of the implantable active-targeting micelle-in-nanofiber device (FM-Nanofiber) and the delivery process of these Dox-loaded micelles (FM) from nanofiber matrix to tumor tissues and finally to tumor cells.

good strategy. By comparison to the systemic administration referred to above, the localized system has some advantages such as ensuring therapeutic drug levels at the tumor site for extended periods of time while maintaining low systemic drug exposure,[22,23] which not only results in higher therapeutic efficacy of the drugs to cancer and a lower toxicity,[24] but also reduces the need for repeat chemotherapeutic administrations, improving the quality of life and enhancing patient compliance.[22] One successful previous study used implantable wafers based on a polyanhydride polymer to locally deliver chemotherapeutic drugs such as carmustine (BCNU) to treat brain cancer.[25] For conventional localized drug delivery systems, the implantable bulk materials (like blocks, films, wafers and so on) and the conventional injectable hydrogel system are the most common forms. For the implantable bulk materials, the degradation rate is hard to be tuned. For the conventional injectable hydrogel systems, which can improve patient compliance and comfort, it can be roughly divided into two categories: particle drug depots and semisolid drug depots.[26] The particle drug depots, including emulsions, liposomes, biodegradable microspheres and micelles, are relatively unstable and easy to migrate away from the tumor site, while, for the semisolid drug depots, the solidification of liquid hydrogel *in vivo* is inconvenient sometimes, and an initial burst of drug may occur during the lag time between the injection and the formation of the solid hydrogel.[26] Currently, the challenges of this localized drug delivery using polymers are the lack of control in drug release and distribution[22] and specific targeting to tumor cells. Therefore, the incorporation of the active targeting micellar system into the implantable, "controllable" matrix may be a good choice to achieve a high chemotherapy efficacy against tumors and low side effects in normal tissues and overcome the drawbacks of the conventional localized drug delivery systems.

In this study, we developed a newly implantable active-targeting micelle-in-nanofiber device for efficient and safe cancer therapy. This device can be achieved as illustrated in Scheme 1. First, the folate-conjugated

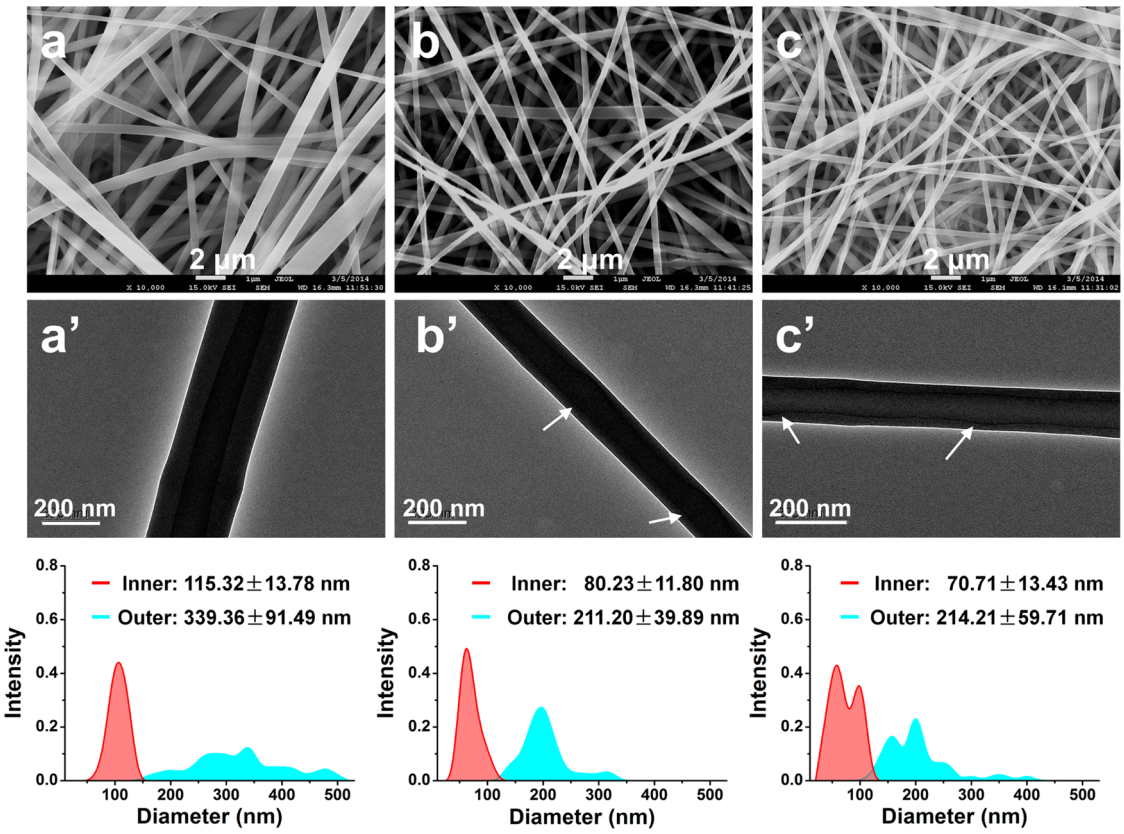

Figure 1. SEM (a−c) and TEM (a′−c′) images of core−shell nanofibers (diameter distributions corresponding to each sample were shown below the images). (a, a′) Gel/PVA nanofiber (outer shell, gelatin, was not cross-linked); (b, b′) FM-Nanofiber; (c, c′) M-Nanofiber. "Slight enlargements" structures were pointed out by white arrows in TEM images.

poly(ε-caprolactone)-poly(ethylene glycol) (FA−PCL-PEG) copolymer were used to encapsulate doxorubicin (Dox), the anticancer drug model, by self-assembling into active-targeting micelles (FM). Folate (FA) ligands can readily bind to the folate receptors (FR) that are overexpressed on the surface of a majority of solid tumors.[27] Later, these micelles are trapped in the core region of the core−shell polymeric nanofibers by coaxial electrospinning in which the inner phase is a blended water solution of poly(vinyl alcohol) (PVA) and the micelles and the outer phase is a gelatin solution. Electrospun fibers are known to be excellent drug carriers with a large surface area to volume ratio and high drug loading and encapsulation efficiency.[28−30] They also have the potential as an implantable device in the tumor or at the surgical resection margins for cancer chemotherapy of solid tumors.[31−33] Subsequently, the resultant nanofiber devices are implanted subcutaneously near the artificial solid tumors. These active-targeting micelles are sustainably released from the devices as a result of the degradation of the nanofiber matrix, rapidly accumulated around the tumor tissue *via* interstitial transport and well-known enhanced permeation and retention (EPR) effect, and specifically internalized by tumor cells *via* FR-mediated endocytosis. The combination of an active-targeting micellar system and an implantable nanofiber device is expected to endow this newly localized drug delivery system with a better performance, *e.g.*, a high therapeutic efficacy, low toxicity, and low treatment costs.

RESULTS AND DISCUSSION

Characterization of the Micelle-in-Nanofiber Devices. To achieve a high encapsulation and protection of the micelles, coaxial electrospinning has been employed to fabricate the implantable active-targeting micelle-in-nanofiber device with a core−shell structure in which Dox-loaded active-targeting micelles mixed with PVA were encapsulated in the core region and genipin cross-linked gelatin formed the outer shell, as shown in Scheme 1. These Dox-loaded micelles were formed by the self-assembly of amphiphilic FA−PEG-PCL and mPEG−PCL copolymers whose compositions and structures were confirmed by ^{1}H NMR (Figure S1a,b in the Supporting Information (SI)). The weight ratio of micelles:PVA was chosen as 1:4 (w/w), under which the electrospinning process was more stable according to our previous work,[34] while the weight ratio of genipin: gelatin was chosen as 3:30 (w/w) based on data illustrated in Figure S2 in SI.

To confirm the core−shell structure of these electrospun nanofibers, SEM and TEM were employed. From the TEM images shown in Figure 1a′−c′, we can identify distinct core−shell structures in the nanofiber

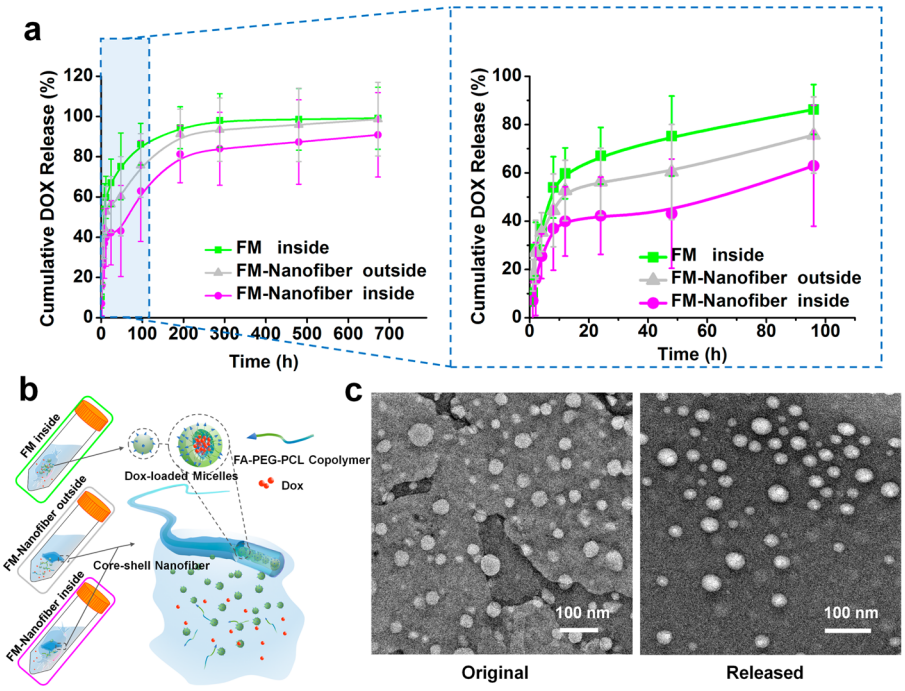

Figure 2. (a) Dox release profiles of FM inside dialysis bag and FM-Nanofiber mats inside and outside of dialysis bag. (b) Scheme of the drug release process. Samples were immersed in phosphate buffered solution (PBS) at pH 7.4. (c) The TEM images of original FM and the released one from nanofibers.

devices, indicating that the coaxial electrospinning was successful. In the SEM images (Figure 1a–c), we observed that all three nanofibers displayed smooth surfaces and uniform diameters. Correspondingly, determination of the diameter distributions showed that the average outer diameters ranged from 339.36 ± 91.49 nm to 211.20 ± 39.89 nm to 214.21 ± 59.71 nm for the Gel_PVA, FM-Nanofiber, and M-Nanofiber samples, while the inner core regions varied from 115.32 ± 13.78 nm to 80.23 ± 11.80 nm to 70.71 ± 13.43 nm, respectively. It appears that both the cross-linking of the outer shell and the introduction of micelles into the inner core contributed to the reduction in diameter. Additionally, after introduction of micelles into PVA core, the diameter of the core became nonuniform and "slight enlargements" can be found in the inner cores of both M-Nanofiber and FM-Nanofiber samples but not in the Gel_PVA samples (Figure 1a′–c′), suggesting that these micelles may be successfully encapsulated into the core regions of the nanofibers.[34]

CLSM was further performed to visualize the micelle distribution in and liberation from the core–shell nanofibers. For observation, Nile red-labeled micelles were also loaded in the nanofiber samples whose outer shells were not cross-linked. In the CLSM images shown in Figure S3a–c in SI, a strong red fluorescence is observed along the axis of the nanofibers, indicating that the Nile red-labeled micelles were successfully embedded in the core–shell nanofibers. After adding a drop of water to the nanofiber mats, no fiber structure could be found in the bright field image (Figure S3d), but lots of red fluorescent spots were found near the nanofibers in the fluorescence image (Figure S3e,f). This was considered to be exposure of the Nile red-labeled micelles due to the fiber matrix dissolution.

***In Vitro* Drug Release.** The release behavior of Dox from single micelles and the implantable micelle-in-nanofiber devices was examined. Figure 2a shows the release profiles of Dox from FM inside dialysis bags and FM-Nanofibers inside and outside dialysis bags. Dox was released from the FM inside dialysis bags as a burst release (~60%) in the first 12 h and had a cumulative release reaching approximately 75% in 48 h and approximately 98% in 288 h. Dox from FM-Nanofibers inside dialysis bags under the same conditions was released as a slight burst release; however, the cumulative release only reached approximately 40% in 48 h and slightly more than 80% in 288 h. A faster Dox release in the single FM group was due to the fact that the thermodynamic stability of the polymeric micelles was susceptible in an aqueous environment.[35] However, after micelles were entrapped in nanofibers, the leaking of the encapsulated drug from the micelles can be prevented by the cross-linked outer shell of the nanofibers, which acts as a barrier and restricts the disassembly of micelles immobilized in the nanofiber matrix (Figure 2b). Thus, encapsulation of Dox-loaded micelles into core–shell nanofibers can prolong the release period of Dox. However, a slight burst release still occurred, which can be ascribed to the fact that the non-cross-linked portion of gelatin in the outer shell and the PVA in the inner core are dissolved in an

aqueous environment because the gel fraction is approximately 85%, as shown in Figure S2. In addition, the Dox release behavior from micelle-dispersed (simply mixed) nanofibers (FM-PVA) (Figure S5) shows a higher burst release and a faster release than the corresponding FM-Nanofibers group (in Figure 2a), which also evidence that the cross-linked outer shell of the nanofiber can prolong the release period of Dox.

To further confirm whether the micelles could be released from the implantable devices, the FM-Nanofiber and M-Nanofiber samples were immersed in DI water at 37 °C for 6 h, and the released micelles (FM or M) were collected and measured as shown in Table S1 in SI. In contrast to the original free micelles, only a minor change in diameter occurs for both FM and M released from the nanofibers. In the TEM images (Figure 2c), the morphologies of the original FM and the released FM were almost the same, with a relatively homogeneous spherical appearance. These results indicated that the micelles could be released from the nanofibers and that the structure of the micelles was not damaged by the electrospinning process.

To understand the release mechanism of Dox from these implantable devices, FM-Nanofiber samples were also placed outside the dialysis bags. As illustrated in Figure 2a and b, we observed a burst release of Dox (over 50%) followed by a slow sustained release (~60% in 48 h and ~90% in 288 h) from FM-Nanofibers outside dialysis bags. The release speed of Dox outside dialysis bags seems to be faster than that of Dox inside dialysis bags. The main reason for this is that both the released Dox and the Dox-loaded micelles were measured for Dox concentration determination when the nanofiber sample was outside of the dialysis bags, leading to an increase in the measured concentration, while only the released Dox was detected when inside dialysis bags.

***In Vitro* Degradation.** Figure S4 in SI reveals the *in vitro* degradation of all the nanofiber devices. The profiles of the Gel_PVA, M-Nanofiber and FM-Nanofiber groups display similar trends in weight loss. After 35 days, the residual weight of the Gel_PVA, M-Nanofiber and FM-Nanofiber mats is less than 5%, which represents an acceptable degradation period without the addition of any enzymes compared to other reports.[36,37] Considering the incomplete cross-linking of the outer shell in the nanofibers, the degradation is mainly attributed to the dissolution of non-cross-linked gelatin and parts of the PVA as well as the release of some micelles at the initial stage. After the initial stage, the weight loss is ascribed to the gradual degradation of the cross-linked outer shell, the dissolution of the inner PVA regions, and the release of more micelles.

Cytotoxicity Assay. Gelatin has excellent biocompatibility and is widely used in the field of biomaterial research. To investigate the cytotoxicity of the implantable micelle-in-nanofiber devices, an Alamar blue assay was performed. Figure S6a in SI exhibits the viability of 4T1 tumor cells and NIH-3T3 fibroblasts treated with blank micelles-in-nanofiber devices in a way that is shown in Figure S6b. For the two cell lines, more than 80% of the cells remain viable after 7 days coculture with the nanofibers. The corresponding fluorescence images (Figure S6c) display that these cells grow healthily, in contrast to the control group. Taken together, these results suggest that the introduction of micelles into gelatin nanofibers does not affect the cytocompatibility of the cells.

Cellular Uptake of Micelles. CLSM and flow cytometry were employed to observe and quantify the intracellular distribution of free Dox-loaded micelles and the released micelles from nanofibers, respectively. As exhibited in Figure S7a, no obvious Dox, as represented by the fluorescence, was observed in the 4T1 cells after incubation with Dox, M, FM, M-Nanofibers and FM-Nanofibers with the same Dox dosage (5 μg/mL) for 0.5 h. However, from the flow cytometry data shown in Figure S7b, we found that after a 0.5-h incubation, the free Dox group showed the highest fluorescence intensity, followed by the FM, M, FM-Nanofibers and M-Nanofibers in descending order. The reason for these differences is mainly ascribed to the fact that free Dox can diffuse directly into cells, which is much faster than the internalization of the other formulations by 4T1 cells. Additionally because the M-Nanofibers and FM-Nanofibers provide a barrier to prolong the release of Dox-loaded micelles, it is not surprising that the micelle-encapsulated nanofiber groups had the lowest fluorescence intensity. After a 4-h incubation, Dox fluorescence inside 4T1 cells was observed in all groups (Figure S7a), and the flow cytometry further verified the enhancement of the fluorescence intensity in cells. The order of fluorescence intensity for all of the groups was not changed in the longer incubation. Taken together, these results suggest that the cellular uptake of the drug and drug-loaded micelles is time-dependent.[38] Additionally, after the micelles are encapsulated into the nanofiber device, the internalization of the micelles into cells could be adjusted through controlling the release of the micelles from the devices.

***In Vitro* Antitumor Effect.** *In vitro* antitumor activity was also evaluated with the Alamar blue assay in 4T1 tumor cells. Here, free Dox, M, and FM were added only once at the beginning of the incubation, whereas the M-Nanofibers and FM-Nanofibers were added in the way shown in Figure 3b. The culture medium was replaced with fresh media without any drug or drug-loaded micelles every 2 days, while the nanofiber samples remained in the wells for the entire incubation time.

Figure 3a shows that the viability of 4T1 cells incubated with the different samples is decreased with incubation time. On day 1, the micelle groups (M and FM) exhibited a lower cell viability than the nanofiber

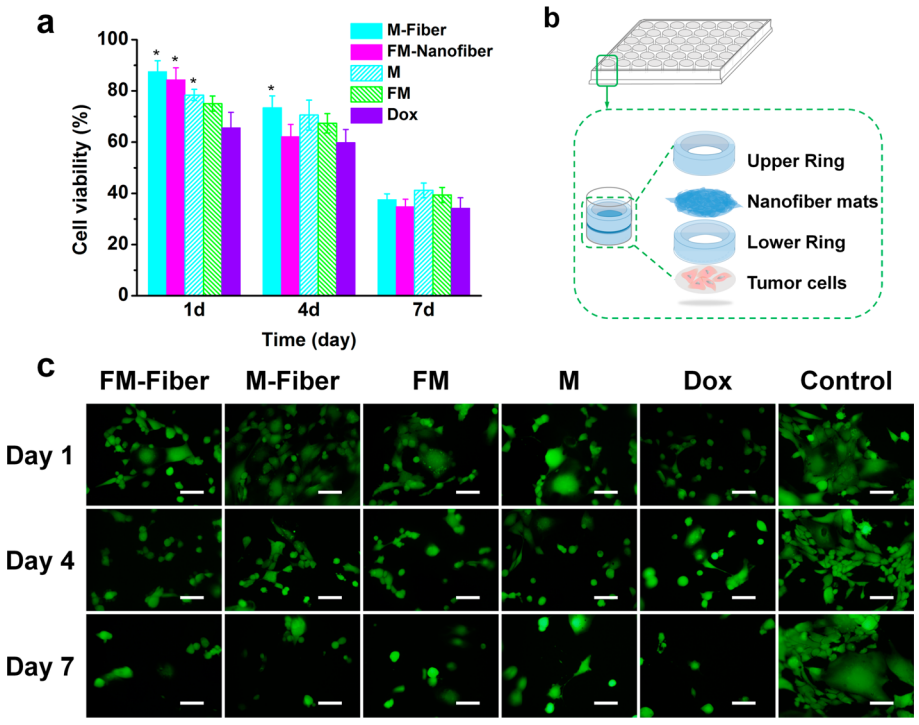

Figure 3. *In vitro* **antitumor activity assay. (a) The viability of 4T1 cells treated by Dox, M, FM, M-Nanofiber and FM-Nanofiber at an equivalent Dox dose of 5 μg/mL for 1, 4, and 7 days. (b) Schematic illustration of the cell culture. The culture medium was replaced with fresh one (without any drugs or micelles) by every 2 days. (c) Corresponding fluorescence images of 4T1 cells treated by different samples. Cells were stained by calcein AM. Scale bar = 50 μm. *$p < 0.05$ *vs* Dox group at the same time point.**

groups, but after 4 days, the cell viability of the FM-Nanofiber group was lower than that of the micelle groups. Furthermore, after incubation for 7 days, the reduction in cell viability in the nanofiber groups is more remarkable than in the micelle groups. According to the *in vitro* Dox release profiles shown in Figure 2a and the cellular uptake analysis shown in Figure S7, we know that at the initial stage in the micelle groups, free Dox and Dox-loaded micelles are abundant in the culture medium and they can easily enter cells by diffusion and internalization, leading to a better antitumor effect than the nanofiber samples. This was also confirmed with a cell apoptosis assay after a 2-d incubation (Figure 4a). After 2-d incubation, the total apoptotic 4T1 cell populations induced by FM and M were 33.5 and 25.3%, respectively, which were slightly higher than that of the FM-Nanofiber (20.6%) and M-Nanofiber (17.6%) groups. However, Dox-loaded micelles were added only once at the beginning of the incubation, and the culture medium of the micelle groups was refreshed every 2 days. Meanwhile, for the nanofiber groups, more and more Dox-loaded micelles were released into the medium with the degradation of the nanofiber matrix. Consequently, after 4 days, the FM-Nanofiber group displayed a lower cell viability than the micelle groups. After 7 days, all groups displayed a lowest cell viability (Figure 3a) and the total apoptotic 4T1 cell populations induced by FM and M were 66.1 and 65.2%, respectively (Figure 4b), which were slightly lower than that of the FM-Nanofiber (69.9%) and M-Nanofiber (67.5%) groups. In addition, the folate-containing groups displayed a better inhibition effect than the nontarget groups, which was believed to be the enhancement of internalization by tumor cells *via* FR-mediated endocytosis.[39,40] Representative fluorescence images shown in Figure 3c agree with these results. Therefore, the implantable active-targeting micelle-in-nanofiber device had the best anticancer efficacy among the groups tested except for the free Dox group. The free Dox group displayed the lowest cell viability, which is ascribed to the fact that free Dox could diffuse quickly into tumor cells after it was added to the culture medium.

***In Vivo* and *Ex Vivo* Dox Fluorescence Imaging.** To visualize the distribution of Dox *in vivo,* solutions including free Dox, M, FM, and saline were injected and the micelle-based nanofiber devices, including FM-Nanofibers and M-Nanofibers, were implanted into 4T1 tumor-bearing nude mice. Dox, represented by fluorescence, was measured at 6, 24, and 48 h in the tumor sites with a Maestro *in vivo* imaging system. Additionally, a pure Dox-loaded nanofiber group (Dox-Nanofiber) was added for further comparison. For all Dox-laden systems, an equivalent amount (1 mg Dox/kg body weight) was applied, which is much less than the dose (5 mg Dox/kg body weight) used in previous reports.[40−43] From the *in vivo* fluorescence images shown in Figure 5a, we observed a weak Dox fluorescence at the tumor sites for all intravenously delivered Dox groups. This result is significantly different from previous reports for

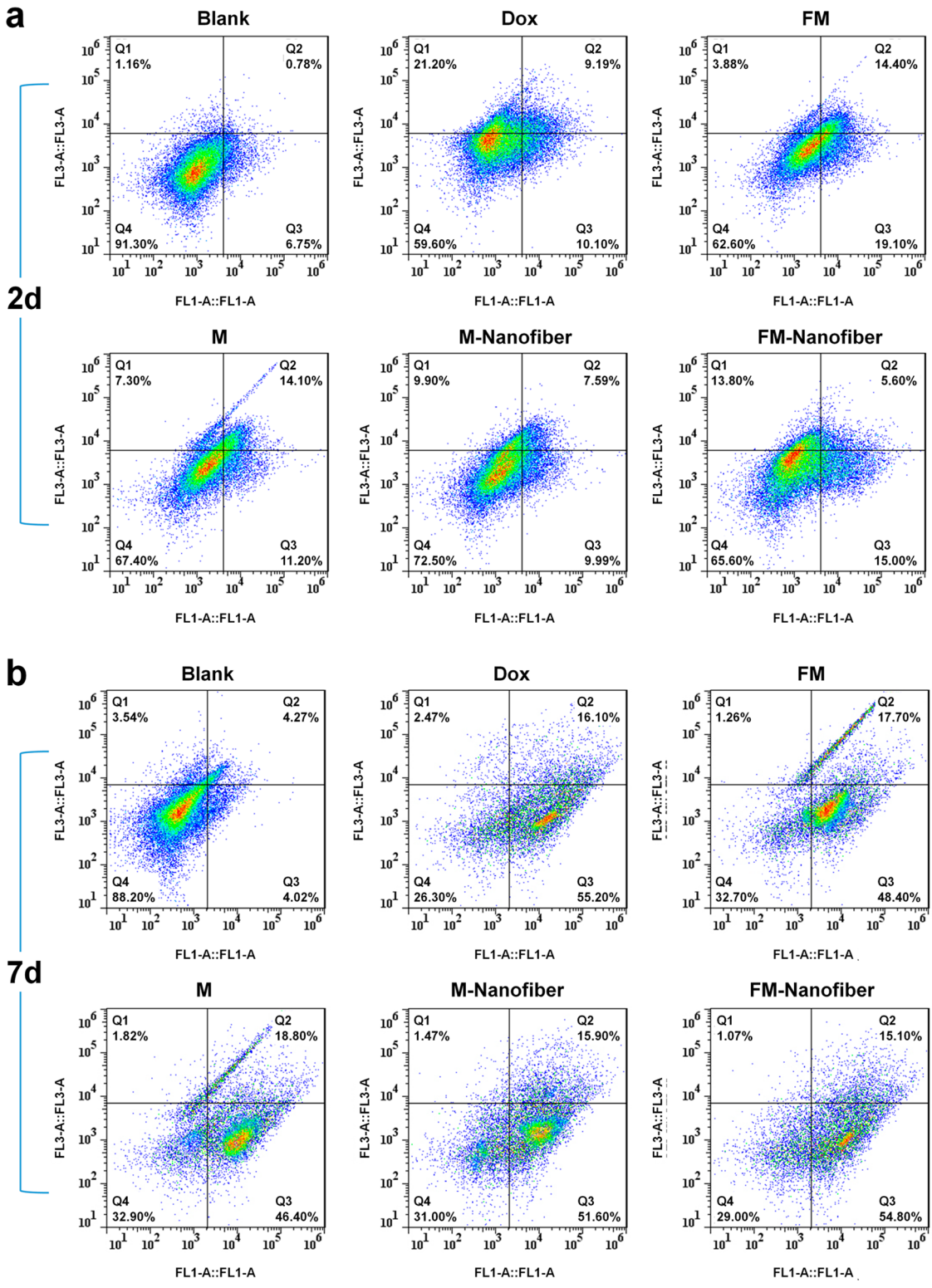

Figure 4. Cell apoptosis of 4T1 cells induced by Dox, M, FM, M-Nanofiber and FM-Nanofiber. Cells were treated with an equivalent Dox dose of 5 μg/mL after (a) 2 days or (b) 7 days incubation and stained with annexin V-FITC and PI for flow cytometry (FCM). The culture medium was replaced with fresh one (without any drugs or micelles) by every 2 days.

Dox-loaded micelles, which have shown a strong fluorescence for up to 24 h after injection with a Dox dosage of 5 mg Dox/kg body weight.[41−43] This difference can be attributed to the low Dox dosage used in this study and the rapid clearance of free micelles from the bloodstream. In contrast to the intravenously delivered Dox groups, the implantable micelle-in-nanofiber devices (M-Nanofiber and FM-Nanofiber groups) and the implantable Dox-Nanofiber group display strong Dox fluorescence near the tumor sites

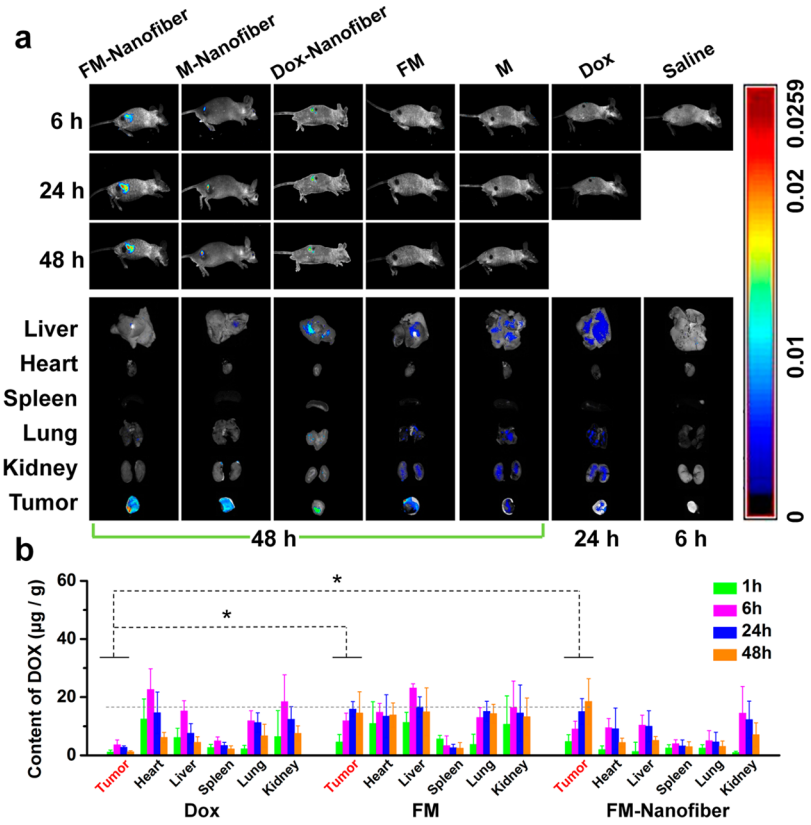

Figure 5. (a) *In vivo* and *ex vivo* Dox fluorescence images showing the Dox biodistribution in nude mice bearing 4T1 murine breast tumor after implantation (FM-Nanofiber and M-Nanofiber) or injection (Dox, M, FM and saline) (Dose: 1 mg Dox/kg body weight) after implantation or injection for different times. (b) Biodistribution in tissues of mice after implantation or injection for different times (Dose: 2 mg Dox/kg body weight). (*$p < 0.05$).

at 6, 24, and 48 h. In addition, the fluorescent region in the implantable groups increases over time, which was an expected result. For the implantable devices implanted near the tumors, initially, the micelles can maintain stability and avoid rapid clearance from the blood circulation due to the immobilization of the nanofibers. With the degradation of the nanofibers *in vivo*, the encapsulated micelles are sustainably released and accumulate rapidly around the tumor tissue *via* interstitial transport including both directly diffusion through the interstitial space and penetration into the blood circulation through the lymphatic system and the subsequent EPR effect, and are finally internalized into the tumor cells by endocytosis (as shown in Scheme 1). Therefore, we observed that the Dox fluorescence in the tumor regions is remarkable and that the intensity increased with time even though the Dox dosage was very low. In addition, the implantable micelle-in-nanofiber devices (M-Nanofiber and FM-Nanofiber groups) displayed a stronger fluorescence near the tumor site than that seen in the Dox-Nanofiber group, suggesting that the micelles, especially the tumor targeting micelles, enhanced the Dox accumulation into the tumor.

At 48 h postadministration, we excised normal tissue and the tumor from the sacrificed mice to directly observe the Dox fluorescence distribution. In the free Dox group, due to the fast elimination of the drug, the tumor and normal tissue were excised at 24 h postinjection. In the saline group, because no fluorescent drug was injected, the tumor and normal tissue were excised at 6 h postadministration. *Ex vivo* imaging determined that the Dox fluorescence was distributed in both the tumor and normal tissue for all intravenously delivered Dox groups (Dox, M and FM); however, in the implantable nanofiber device groups (M-Nanofiber and FM-Nanofiber), the fluorescence was mainly concentrated in the tumors with only a small amount distributed in the normal tissue, suggesting that the localized delivery of Dox is highly effective at targeting the accumulation of most of the anticancer agent in the tumor tissue. Meanwhile, the Dox fluorescence was observed in both the tumor and the liver in the Dox-Nanofiber group. Additionally, the implantable active-targeting micelle-in-nanofiber device displays the strongest fluorescent intensity at the tumor site, indicating that the released micelles are specifically internalized into tumor cells *via* receptor-mediated endocytosis. Therefore, this implantable device has the ability of ensuring therapeutic drug levels at the tumor site for extended periods of time while maintaining low systemic drug exposure to the normal tissue. It is obviously superior to the commonly used method of intravenously delivered therapeutic agents

in which a minimal amount of drugs reaches the tumor site.[42−44]

***In Vivo* Biodistribution.** For further confirmation, the amount of accumulated Dox in the tumors and major tissues of tumor-bearing Balb/C mice at 1, 6, 24, and 48 h postadministration was measured in the intravenously delivered free Dox, the active-targeting micelles (FM), and the implantable nanofiber device (FM-Nanofiber) groups. The level of Dox was determined by fluorescence spectroscopy as shown in Figure 5b. Considering that the fluorescence was weak for the free Dox and FM groups in the *in vivo* and *ex vivo* Dox fluorescence imaging illustrated in Figure 5a due to a low dosage of Dox, we slightly increased the Dox dosage of each group to 2 mg Dox/kg body weight, which was still much lower than that reported previously (5−10 mg Dox/kg body weight).[44−51] As shown in Figure 5b, after injection or implantation for 1, 6, 24, and 48 h, the Dox accumulation in the tumors of the FM and FM-Nanofiber groups was significantly higher than that of the free Dox group. This was because the micellar carrier with a bulky hydrophilic outer shell allowed the drug to evade specific recognition by the reticuloendothelial system (RES).[52] In addition, the EPR effect in the tumor tissue, which has tortuous and leaky vasculature,[53] could contribute to the enrichment of the drug in the tumor. The micelles were also functionalized with folate, which enhanced the targeting effect.[39] The main accumulation of Dox in the normal tissue was detected in the heart, liver, lung and kidney. The FM-Nanofiber group had a lower accumulation of Dox in those organs than the other groups (Dox and FM), which confirmed that this implantable local drug delivery system, specifically micelles encapsulated in nanofibers, was capable of limiting the distribution of the drug in normal organs. Furthermore, the accumulation of Dox in the tumors of the FM-Nanofiber group was higher than that of the FM group after 48 h, suggesting that this implantable device has the ability to ensure therapeutic drug levels at the tumor site for extended periods of time.

***In Vivo* Antitumor Effect.** Figure 6a, b illustrate the antitumor effect of the intravenously delivered formulations and the implantable nanofiber devices after being applied to 4T1 tumor-bearing Balb/c mice. After 21 days, the mean tumor volume of nanofiber groups is smaller than that of intravenously delivered Dox formulations groups. The variation in tumor volume demonstrates that although without a significant difference in the anticancer efficacy between nanofiber groups and the intravenously delivered Dox formulation groups, the only once implantation of nanfiber groups, especially the active-targeting micelle-in-nanofiber device (FM-Nanofiber), have displayed a comparable tumor growth suppression compared with the four times injection of Dox, M or FM groups after 21 days of treatment. This can be ascribed to an enrichment of the released anticancer drug and micelles at the tumor site with the degradation of the nanofiber matrix, ensuring therapeutic drug levels at the tumor site for an extended period (Figure 5a). This is also evidenced by the *in vivo* degradation of the implantable devices for 1 and 11 days. From the morphologies of these nanofibers, shown in Figure S8, we observed that the nanofibers swelled and started to break after 1 day and that no fiber-like structures could be found after 11 days, suggesting that these devices possessed a good biodegradability. Therefore, by the degradation of the nanofiber, the encapsulated micelles can be sustainably released.

Additionally, the intravenously delivered free Dox and Dox-loaded micelles (M and FM) exhibit a weaker anticancer efficacy than the corresponding formulations reported previously,[40,41,44,46,47] which is mainly due to the low Dox dosage (2 mg/kg used in this study and the rapid clearance of drug in the blood circulation. This is also evidenced by the *in vivo* and *ex vivo* Dox fluorescence imaging shown in Figure 5a. It is noted that even though the intravenously delivered Dox formulations were injected 4 times (total Dox dosage: 8 mg/kg) and the nanofiber devices were implanted only once (2 mg/kg) for this cancer treatment, the implantable device groups still displayed comparable anticancer efficacy, further indicating that this localized delivery system could reduce the drug loss caused by the RES[20] and could maintain therapeutic drug levels at the tumor site for extended periods of time. For comparison, the formulations of F, FM, or Dox were injected once to 4T1 tumor-bearing Balb/c mice at an equivalent Dox dose of 2 mg/kg in the very beginning of the treatment and the corresponding data were shown in Figure S9. We can find that after 21 days, the mean tumor volumes of all the groups were over 1000 mm^3, which were much larger than the nanofiber groups (less than 500 mm^3) in Figure 6. The result suggests that under the same dosage of Dox (2 mg/kg), nanofiber groups performed much better antitumor effect than the once-injection of micelles or Dox alone groups. On the other hand, the implantable nanofiber devices, especially the FM-Nanofiber group, also maintain low systemic drug exposure to the normal tissue, resulting in a slight increase in body weight (Figure 6c), and a high survival rate (Figure 6d) for these treated mice in contrast to the saline group, blank-nanofiber group and the once-injection groups (Figure S9). These results also demonstrate that the localized drug delivery system of the implantable micelle-in-nanofiber device possesses a high therapeutic efficacy against tumors and a low toxicity to the body.

To further confirm the therapeutic efficacy, histological analysis of tumor sections was performed 21 days after the first injection or implantation. From the H&E stained images shown in Figure 6e, we found that all

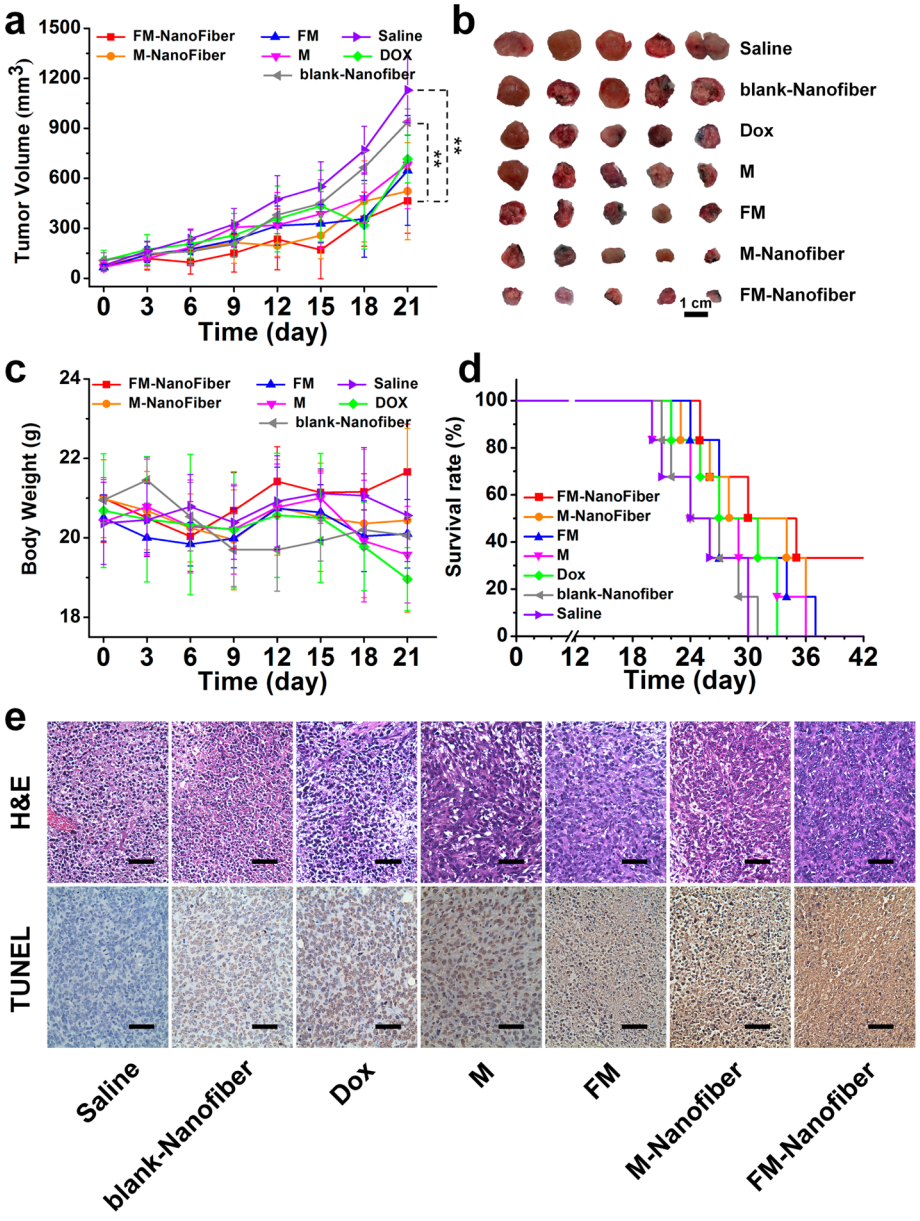

Figure 6. *In vivo* **antitumor effect and systemic toxicity of Dox, M, FM, M-Nanofiber and FM-Nanofiber. The artificial 4T1 murine breast cancer model was established at the lower right flank of the Balb/C mice subcutaneously as tumor models. (a) Changes of tumor volume. (b) Excised 4T1 solid tumors from different treatment groups at the day 21. (c) The body weight and (d) survival rate of tumor-bearing Balb/C mice receiving different treatment. (e) H&E staining and TUNEL analysis of tumor sections at the day 21 after the first treatment. (Scale bars = 200 μm). The intravenous administration of Dox and Dox-loaded micelles (M and FM) was performed every 2 days for a total of 4 times at an equivalent Dox dose of 2 mg/kg for each time. M-Nanofiber and FM-Nanofiber were implanted only once in the beginning at an equivalent Dox dose of 2 mg/kg. (*$p < 0.05$ and **$p < 0.01$).**

Dox-containing groups exhibited apoptosis, which was characterized by the cells becoming smaller, lysis of the nuclei, the appearance of vacuoles, and the destruction of membrane integrity, especially for the M-Nanofiber and FM-Nanofiber groups. Apoptotic cells, which appeared dark brown, were also identified with a TUNEL assay. In the FM-Nanofiber group, nuclear membrane cracking and chromatin condensation, marginalization and division into blocks or apoptotic bodies, which is an obvious sign of apoptosis of tumor cells as reported previously,[54,55] were clearly observed. The mean optical density (OD) values were quantitatively determined from TUNEL staining and are illustrated in Figure S10 in SI. The apoptosis rate (OD value 0.24 $\pm$ 0.01) of the tumor cells in the FM-Nanofiber group is the highest and is significantly increased compared with the other groups, which indicates the excellent superiority of this device in suppressing the growth of tumor cells.

CONCLUSION

In summary, we have successfully developed a new localized drug delivery device by incorporation of

active-targeting micellar system into implantable polymeric nanofibers. Although there are some limitations for this new implantable device, like that a surgical operation must be done when using it, and it is not easy to achieve a reproducible production on a massive scale since the coaxial electrospinning process is governed by many parameters, it is still a promising tool to treat cancers. Compared to the commonly used delivery strategy of repeatedly intravenous injections of micelles for cancer therapy, this implantable device, loaded with a low dosage of a therapeutic agent, has the ability to ensure therapeutic drug levels at the tumor site for extended periods of time while maintaining low systemic drug exposure to normal tissue. Meanwhile, the specific internalization of these micelles into the tumor cells can be further achieved by receptor-mediated endocytosis, leading to a high therapeutic efficacy against tumor cells and a low toxicity to normal tissue. Moreover, this implantable device system greatly reduces the frequency of drug administration, which can potentially improve the quality of life and enhance compliance of the patient. To the best of our knowledge, this is the first report dealing with the use of an implantable active-targeting micelle-in-nanofiber device for the treatment of cancer. This study opens a wide range of new possibilities for the development of multifunctional implantable devices for effective and safe cancer therapy.

MATERIALS AND METHODS

Materials. Folic acid (FA), poly(ethylene glycol) (PEG, M_n = 2.0 kDa), poly(vinyl alcohol) (PVA, number-average degree of polymerization of 1700, degree of saponification: 88%) and gelatin powder (type A, from porcine skin) were purchased from Chengdu Kelong Chemical Reagent Company (China). ε-Caprolactone (ε-CL, Aldrich) was dried over CaH_2 overnight and distilled at reduced pressure before use. Monomethyl poly(ethylene glycol) (mPEG, M_w = 2.0 kDa), 1-Ethyl-3-(3-dimethylaminopropyl) carbodiimide hydro-chloride (EDC·HCl), *N*-hydroxysuccinimide (NHS), 4′, 6-diamidino-2-phenylindole, dihydrochloride (DAPI) were purchased from Sigma-Aldrich (USA). The FA-conjugated copolymer FA−PEG-PCL and mPEG−PCL copolymer were synthesized as illustrated in Scheme S1 in SI as our previous reports.[40,56] Doxorubicin hydrochloride (Dox·HCl) was purchased from Zhejiang Hisun Pharmaceutical Co., Ltd. (China). Nile red (Acros) was obtained from Shanghai Titan technology Co., Ltd. Annexin V-FITC Apoptosis Detection Kits were purchased from Nanjing KeyGEN Biotech (China) and used as received. All other chemicals with reagent grade or better were obtained from commercial sources and used without further purification. Deionized (DI) water was used in all experiments.

Preparation of Blank and Dox/Nile Red-Loaded Micelles. A solvent evaporation method was employed to fabricate the blank and Dox-loaded micelles with FA−PEG-PCL and mPEG−PCL copolymers. Briefly, blank micelles of two different copolymers were fabricated by dropwise addition of 10.0 mL of block copolymer solution in tetrahydrofuran (THF) to 10.0 mL of deionized water under stirring, followed by the evaporation of THF at room temperature. Hydrophobic drug doxorubicin (Dox) obtained from Dox·HCL with the aid of triethylamine was used as model drug to prepare the Dox-loaded micelles. The same procedures were carried out as mentioned above, except that all processes were operated in the dark. After the THF was evaporated completely, the Dox-loaded micelles were transferred into dialysis bag (MWCO 1000) with distilled water to remove the unloaded Dox. Finally, both of the blank and Dox-loaded micelles were lyophilized and stored at −20 °C for future use. To clearly observe the micelles in polymer fibers, Nile red, which has strong red fluorescence, was encapsulated into polymer micelles by the similar method mentioned above and the unloaded one was removed by centrifugation.

Characterization of Micelles. For further characterization, all samples with a concentration of 1.00 mg/mL were filtered with a 0.22-μm syringe filter before measurement. The diameter of micelles was determined with a dynamic light scattering (DLS) measurement device with a Malvern Zetasizer Nano-ZS90 apparatus. The morphologies of the micelles were observed by transmission electron microscopy (TEM) (JEOL 2100F, JEOL, Ltd., Japan). Drug loading content (LC) and encapsulation efficiency (EE) of Dox-loaded micelles were measured with a UV−vis spectrophotometer (UV-2550, Shimadzu, Japan).

The investigated micellar samples were labeled as follows: M (Dox-loaded micelles fabricated from an mPEG−PCL copolymer) and FM (Dox-loaded micelles fabricated from an FA−PEG-PCL copolymer). Unless otherwise specified, all micelles were Dox-loaded micelles.

Electrospinning of Micelle-in-Nanofiber Devices. To fabricate the micelle-in-nanofiber devices, a homemade coaxial metal needle was used. The inner diameter of the outer needle was 0.9 mm, and the inner and outer diameter of the inner needle were 0.33 and 0.63 mm, respectively. The inner fluid was a 12.5% (w/v) blended solution of PVA and micelles (4:1, w/w) in DI water. The outer fluid was a 22% (w/v) blended solution of gelatin and genipin (30:3, w/w) in a mixture of acetic acid/DI water (9:1, v/v). Before electrospinning, the outer fluid was stirred for over 8 h to cross-link the gelatin with the genipin. The flow rates of the outer and inner fluids were fixed at 0.15 mL/h by a microinjection pump (LSP02−1B, LongerPump, China). The distance between the needles and the collector (aluminum foil) was 14 cm, and a constant 22 kV electric potential was applied. A pure Dox-loaded coaxial nanofiber (Dox-Nanofiber) was also fabricated by replacing the inner fluid with a blended solution of PVA and Dox·HCL.

The investigated micelle-in-nanofiber device samples were labeled as follows: M-Nanofiber (Dox-loaded micelles encapsulated in a coaxial nanofiber), FM-Nanofiber (Dox-loaded FA-decorated micelles encapsulated in a coaxial nanofiber), Dox-Nanofiber (Dox·HCL encapsulated in a coaxial nanofiber), blank-Nanofiber (blank micelles encapsulated in a shell-cross-linked coaxial nanofiber), Gel (a genipin-cross-linked pure gelatin nanofiber), Gel_PVA (a shell-cross-linked coaxial nanofiber without micelles), Gel/PVA nanofiber (a coaxial nanofiber without encapsulated micelles) and FM-PVA (fabricated by electrospinning the blend of blended solution of PVA and FM (4:1, w/w)).The outer shells of all of the described nanofibers, except the Gel/PVA nanofiber and FM-PVA nanofiber, were cross-linked with genipin at a weight ratio of 3:30 (genipin:gelatin, w/w). Without special declaration, all nanofibers used in the study were cross-linked with genipin at a weight ratio of 3:30 (genipin:gelatin, w/w).

Characterization of the Micelle-in-Nanofiber Device. The surface morphologies and core−shell structures of the nanofibers were observed with a field emission scanning electron microscope (FE-SEM) (JSM-7001F, JEOL, Ltd. Japan) and a TEM (JEOL 2100F, JEOL, Ltd. Japan), respectively. The SEM samples were prepared by coating a thin layer of platinum onto the nanofiber mats. Prior to TEM imaging, samples were collected onto a copper grid covered with a carbon film. ImageJ software (1.46 h, NIH, USA) was used to analyze three randomly selected areas of images taken from each SEM sample or TEM sample, and the inner/outer diameter distribution of coaxial nanofibers was counted.

Confocal laser scanning microscopy (CLSM) (Olympus FV1000) was applied to visualize the distribution of micelles

inside the nanofibers. For observation, Nile red-labeled micelles were prepared and electrospun into the core region of the core−shell nanofibers in which the outer shell was not cross-linked. The nanofiber samples were all collected onto coverslips and placed upside down on another glass coverslip. Samples under both dry and wet conditions were observed. The samples in the wet state were prepared by adding a drop of DI water to one side of the gap between the glass coverslips so that the water could infiltrate the nanofibers.

***In Vitro* Release of Micelles from the Micelle-in-Nanofiber Devices.** To determine the amount of micelles released from the micelle-encapsulated coaxial nanofibers, the FM-Nanofiber mats were immersed in DI water at 37 °C in a thermostated incubator with a shaking speed of 100 rpm. After approximately 6 h, the solution containing released micelles was collected. The amount of released micelles was measured with DLS and observed with TEM.

***In Vitro* Drug Release and Fiber Matrix Degradation.** The *in vitro* release kinetics of Dox from Dox-loaded micelles, micelle-in-nanofiber devices and FM-PVA nanofibers were investigated in phosphate buffer saline (PBS, pH 7.4). The freeze-dried Dox-loaded micelles were diluted to 1 mg/mL, and 1.0 mL of this solution was transferred to a dialysis bag (MWCO 1000). The bag was then immersed into a tube containing 30 mL of incubation media at 37 °C and maintained in a thermostated incubator with a shaking speed of 100 rpm. The amount of released Dox in the incubation medium was quantified with a fluorescence spectrophotometer (F-7000, Hitachi, Japan).[40] The degradation of nanofibers (M-Nanofibers, FM-Nanofibers, Gel and Gel_PVA) was measured as follows: the dried nanofiber mats were cut into small pieces, and each sample (approximately 10 mg at initial weight) was immersed in 10 mL PBS (pH 7.4) with the same conditions as the release experiment. At each preset time point, samples were dried and weighed.

Cytotoxicity Assay. The cytotoxicity assay, based on the Alamar blue assay, was carried out on 4T1 cells (tumor cells) and NIH 3T3 fibroblasts (normal cells). Cells were seeded into 48-well plates at a density of 1×10^4 cells/well. After the cells attached and were well spread, the blank micelle-encapsulated coaxial nanofiber mats were immersed in the culture medium and fixed between two rings.[34] The culture medium was refreshed every 2 days. At 1, 4, and 7 day time points, an Alamar blue assay was performed and an ELISA microplate reader (Molecular Devices, Sunnyvale, CA) was used to read the absorbance of the Alamar blue solution at 570 nm (excitation)/600 nm (emission) after a 4-h incubation. Meanwhile, cells were stained with 1 μM calcein AM (Sigma, USA) and observed with fluorescence microscopy (CKX41, Olympus, Japan) at each time point.

Evaluation of the Cellular Uptake of Micelles. The cellular uptake of micelles was evaluated with CLSM and flow cytometry (FCM) with a flow cytometer (BD AcCuri C6, USA). For CLSM observation, cells were seeded onto coverslips in 6-well plates and cultured with different micellar samples with an equivalent Dox dosage of 5 μg/mL for 0.5 and 4 h. Then, the cells were fixed with 2.5% glutaraldehyde for 50 min and stained with DAPI for 7 min. For FCM analysis, at each preset time point, cells were treated with trypsin and centrifuged at 2000 rpm for 3 min to collect the cells. Then, the flow cytometer was used to analyze the fluorescence intensity of the collected cells.

***In Vitro* Antitumor Activity and Cell Apoptosis Assay.** The *in vitro* antitumor activity of Dox-loaded micelles (M and FM) and Dox- and micelle-encapsulated Nanofiber mats (M-Nanofibers and FM-Nanofibers) was based on the Alamar blue assay in 4T1 cells. The initial cell density was 2×10^4 cells/well in 48-well plates and experimental procedure were the same as mentioned in Cytotoxicity Assay. All samples were added at an equivalent Dox dosage of 5 μg/mL. The culture medium was replaced with fresh one (without any drugs or micelles) by every 2 days.

To confirm the therapeutic effect of each sample, the cell apoptosis assay was assessed with FCM. 4T1 cells were seeded in 6-well plates at a density of 1×10^5 cells/well. After cell attachment, Dox-loaded micelles (M and FM) and Dox- and micelle-encapsulated Nanofiber mats (M-Nanofibers and FM-Nanofibers) were added at an equivalent Dox dosage of 5 μg/mL to the cells, and samples were incubated for 48 h. Then, the rate of apoptosis was measured using an Annexin V-FITC Apoptosis Detection Kit in compliance with the manufacturer's protocol.

***In Vivo* and *Ex Vivo* Dox Fluorescence Imaging.** Saline, Dox and Dox-loaded micelles (M and FM) were injected into 4T1 tumor-bearing nude mice *via* the lateral tail vein at a 1 mg/kg equivalent Dox dosage. The micelle-in-nanofiber devices (M-Nanofiber and FM-Nanofiber) with the same Dox dosage (1 mg/kg) were implanted subcutaneously near the tumors. At 6, 24, or 48 h postinjection, the mice were anesthetized and imaged with a Maestro *in vivo* imaging system. At 6 and 24 h, the saline and Dox group mice were sacrificed and the tissues were imaged. At 48 h, mice from all four groups (M, FM, M-Nanofiber and FM-Nanofiber) were sacrificed, and the normal organs as well as tumors were also imaged.

***In Vivo* Antitumor Effect and Drug Biodistribution Study.** Approximately 10 days postinoculation of 4T1 cells, tumors in the Balb/C mice were detachable and reached a volume of approximately 50 mm^3 (labeled as 0 day). Mice were randomly divided into six groups (n = 6). Then, saline, Dox and Dox-loaded micelles (M and FM) were administered intravenously into the 4T1 tumor-bearing nude mice at a 2 mg/kg equivalent Dox dosage. Meanwhile, the micelle-in-nanofiber devices with a Dox dosage of 2 mg/kg were implanted subcutaneously near the tumors. The intravenous administration of saline, Dox and Dox-loaded micelles (M and FM) was performed every 2 days for a total of 4 times. The weight and size of the tumors in all mice were recorded every 2 days following the initial treatment.

The Dox, FM and FM-Nanofiber groups were further used to evaluate the biodistribution of the drug. Tumor-bearing mice were randomized into three groups (n = 3) and were injected intravenously with the Dox or FM solutions or implanted subcutaneously with the FM-Nanofiber device at a Dox dosage of 2 mg/kg. At the indicated time intervals, normal organs (heart, liver, spleen, lung, and kidney) and tumor tissue were collected from the mice. Tissue samples were rinsed in saline, wiped with filter paper, weighed and then stored at −20 °C until undergoing analysis. The fluorescence of the samples was measured. The tissue distribution of Dox was expressed as the amount of Dox per gram of tissue.

Histological Examination. At day 21, tumor tissues of portions of mice were collected in 4% formaldehyde and embedded in paraffin blocks after dehydrating with gradient ethanol. Then tissue sections were stained with hematoxylin/eosin (H&E) or Terminal deoxynucleotidyl transferase dUTP nick end labeling (TUNEL) for microscopic observation. The mean optical density (OD) values were measured from three pictures of each sample with Image-Pro Plus 6.0 software.[16]

Statistics Analysis. All experiments were performed in triplicate or more specimens. The results were shown as mean ± standard deviation. Single factorial analysis of variance (ANOVA) was performed to determine statistical significance of the data.

Conflict of Interest: The authors declare no competing financial interest.

Acknowledgment. This work was partially supported by National Basic Research Program of China (973 Program, 2012CB933600), National Natural Science Foundation of China (Nos. 30970723, 51173150, 51373138), Research Fund for the Doctoral Program of Higher Education of China (20120184110029), Construction Program for Innovative Research Team of University in Sichuan Province (14TD0050) and the 2014 Doctoral Innovation Funds of Southwest Jiaotong University and the Fundamental Research Funds (SWJTU11ZT10, 2682013CX001) for the Central Universities.

Supporting Information Available: Cell lines and culture conditions and animals. Additional figures including Scheme S1, Figure S1−S10 and Table S1 as described in the text. This material is available free of charge *via* the Internet at http://pubs.acs.org.

REFERENCES AND NOTES

1. Langer, R. Drug Delivery and Targeting. *Nature* **1998**, *392*, 5–10.

2. Minchinton, A. I.; Tannock, I. F. Drug Penetration in Solid Tumours. *Nat. Rev. Cancer* **2006**, *6*, 583–592.
3. Jemal, A.; Siegel, R.; Ward, E.; Murray, T.; Xu, J. Q.; Smigal, C.; Thun, M. J. Cancer Statistics, 2006. *CA-Cancer J. Clin.* **2006**, *56*, 106–130.
4. O'Gorman, C.; Sasiadek, W.; Denieffe, S.; Gooney, M. Predicting Radiotherapy-Related Clinical Toxicities in Cancer: a Literature Review. *Clin. J. Oncol. Nurs.* **2014**, *18*, E37–E44.
5. Moses, M. A.; Brem, H.; Langer, R. Advancing the Field of Drug Delivery: Taking Aim at Cancer. *Cancer Cell* **2003**, *4*, 337–341.
6. Ferrari, M. Cancer Nanotechnology: Opportunities and Challenges. *Nat. Rev. Cancer* **2005**, *5*, 161–171.
7. Peer, D.; Karp, J. M.; Hong, S.; FaroKhzad, O. C.; Margalit, R.; Langer, R. Nanocarriers as an Emerging Platform for Cancer Therapy. *Nat. Nanotechnol.* **2007**, *2*, 751–760.
8. Farokhzad, O. C.; Langer, R. Impact of Nanotechnology on Drug Delivery. *ACS Nano* **2009**, *3*, 16–20.
9. Newland, B.; Zheng, Y.; Jin, Y.; Abu-Rub, M.; Cao, H. L.; Wang, W. X.; Pandit, A. Single Cyclized Molecule *Versus* Single Branched Molecule: A Simple and Efficient 3D "Knot" Polymer Structure for Nonviral Gene Delivery. *J. Am. Chem. Soc.* **2012**, *134*, 4782–4789.
10. Kazunori, K.; Glenn, S. K.; Masayuki, Y.; Teruo, O.; Yasuhisa, S. Block Copolymer Micelles as Vehicles for Drug Delivery. *J. Controlled Release* **1993**, *24*, 119–132.
11. Fox, M. E.; Szoka, F. C.; Frechet, J. M. J. Soluble Polymer Carriers for the Treatment of Cancer: The Importance of Molecular Architecture. *Acc. Chem. Res.* **2009**, *42*, 1141–1151.
12. Wang, C.; Wang, Z. Q.; Zhang, X. Amphiphilic Building Blocks for Self-Assembly: From Amphiphiles to Supra-Amphiphiles. *Acc. Chem. Res.* **2012**, *45*, 608–618.
13. Nicolas, J.; Mura, S.; Brambilla, D.; Mackiewicz, N.; Couvreur, P. Design, Functionalization Strategies and Biomedical Applications of Targeted Biodegradable/Biocompatible Polymer-Based Nanocarriers for Drug Delivery. *Chem. Soc. Rev.* **2013**, *42*, 1147–1235.
14. Allen, T. M.; Cullis, P. R. Drug Delivery Systems: Entering the Mainstream. *Science* **2004**, *303*, 1818–1822.
15. Basarkar, A.; Singh, J. Poly(lactide-co-glycolide)-Polymethacrylate Nanoparticles for Intramuscular Delivery of Plasmid Encoding Interleukin-10 to Prevent Autoimmune Diabetes in Mice. *Pharm. Res.* **2009**, *26*, 72–81.
16. Wang, J.; Yang, G.; Guo, X.; Tang, Z. M.; Zhong, Z. D.; Zhou, S. B. Redox-Responsive Polyanhydride Micelles for Cancer Therapy. *Biomaterials* **2014**, *35*, 3080–3090.
17. Alonso, M. J. Nanomedicines for Overcoming Biological Barriers. *Biomed. Pharmacother.* **2004**, *58*, 168–172.
18. Couvreur, P.; Vauthier, C. Nanotechnology: Intelligent Design to Treat Complex Disease. *Pharm. Res.* **2006**, *23*, 1417–1450.
19. Petros, R. A.; DeSimone, J. M. Strategies in the Design of Nanoparticles for Therapeutic Applications. *Nat. Rev. Drug Discovery* **2010**, *9*, 615–627.
20. Koo, H.; Huh, M. S.; Sun, I. C.; Yuk, S. H.; Choi, K.; Kim, K.; Kwon, I. C. *In Vivo* Targeted Delivery of Nanoparticles for Theranosis. *Acc. Chem. Res.* **2011**, *44*, 1018–1028.
21. Albanese, A.; Tang, P. S.; Chan, W. C. W. The Effect of Nanoparticle Size, Shape, and Surface Chemistry on Biological Systems. *Annu. Rev. Biomed. Eng.* **2012**, *14*, 1–16.
22. De Souza, R.; Zahedi, P.; Allen, C. J.; Piquette-Miller, M. Polymeric Drug Delivery Systems for Localized Cancer Chemotherapy. *Drug Delivery* **2010**, *17*, 365–375.
23. Wolinsky, J. B.; Colson, Y. L.; Grinstaff, M. W. Local Drug Delivery Strategies for Cancer Treatment: Gels, Nanoparticles, Polymeric Films, Rods, and Wafers. *J. Controlled Release* **2012**, *159*, 14–26.
24. Ho, E. A.; Soo, P. L.; Allen, C.; Piquette-Miller, M. Impact of Intraperitoneal, Sustained Delivery of Paclitaxel on the Expression of P-glycoprotein in Ovarian Tumors. *J. Controlled Release* **2007**, *117*, 20–27.
25. Brem, H.; Piantadosi, S.; Burger, P. C.; Walker, M.; Selker, R.; Vick, N. A.; Black, K.; Sisti, M.; Brem, S.; Mohr, G.; *et al.* Placebo-Controlled Trial of Safety and Efficacy of Intraoperative Controlled Delivery by Biodegradable Polymers of Chemotherapy for Recurrent Gliomas. The Polymer-Brain Tumor Treatment Group. *Lancet* **1995**, *345*, 1008–1012.
26. Hatefi, A.; Amsden, B. Biodegradable Injectable *In Situ* Forming Drug Delivery Systems. *J. Controlled Release* **2002**, *80*, 9–28.
27. Low, P. S.; Kularatne, S. A. Folate-Targeted Therapeutic and Imaging Agents for Cancer. *Curr. Opin. Chem. Biol.* **2009**, *13*, 256–262.
28. Chakraborty, S.; Liao, I. C.; Adler, A.; Leong, K. W. Electrohydrodynamics: a Facile Technique to Fabricate Drug Delivery Systems. *Adv. Drug Delivery Rev.* **2009**, *61*, 1043–1054.
29. Szentivanyi, A.; Chakradeo, T.; Zernetsch, H.; Glasmacher, B. Electrospun Cellular Microenvironments: Understanding Controlled Release and Scaffold Structure. *Adv. Drug Delivery Rev.* **2011**, *63*, 209–220.
30. Joshi, M.; Butola, B. S.; Saha, K. Advances in Topical Drug Delivery System: Micro to Nanofibrous Structures. *J. Nanosci. Nanotechnol.* **2014**, *14*, 853–867.
31. Kim, Y.; Ebara, M.; Aoyagi, T. A Smart Hyperthermia Nanofiber with Switchable Drug Release for Inducing Cancer Apoptosis. *Adv. Funct. Mater.* **2013**, *23*, 5753–5761.
32. Ranganath, S. H.; Wang, C. H. Biodegradable Microfiber Implants Delivering Paclitaxel for Post-Surgical Chemotherapy Against Malignant Glioma. *Biomaterials* **2008**, *29*, 2996–3003.
33. Ranganath, S. H.; Fu, Y.; Arifin, D. Y.; Kee, I.; Zheng, L.; Lee, H. S.; Chow, P. K.; Wang, C. H. The Use of Submicron/Nanoscale PLGA Implants to Deliver Paclitaxel with Enhanced Pharmacokinetics and Therapeutic Efficacy in Intracranial Glioblastoma in Mice. *Biomaterials* **2010**, *31*, 5199–5207.
34. Yang, G.; Wang, J.; Li, L.; Ding, S.; Zhou, S. B. Electrospun Micelles/Drug-Loaded Nanofibers for Time-Programmed Multi-Agent Release. *Macromol. Biosci.* **2014**, *14*, 965–976.
35. Owen, S. C.; Chan, D. P. Y.; Shoichet, M. S. Polymeric Micelle Stability. *Nano Today* **2012**, *7*, 53–65.
36. Cao, L.; Werkmeister, J. A.; Wang, J.; Glattauer, V.; McLean, K. M.; Liu, C. Bone Regeneration Using Photocrosslinked Hydrogel Incorporating rhBMP-2 Loaded 2-N, 6-O-Sulfated Chitosan Nanoparticles. *Biomaterials* **2014**, *35*, 2730–2742.
37. Koshy, S. T.; Ferrante, T. C.; Lewin, S. A.; Mooney, D. J. Injectable, Porous, and Cell-Responsive Gelatin Cryogels. *Biomaterials* **2014**, *35*, 2477–2487.
38. Yan, Y.; Johnston, A. P. R.; Dodds, S. J.; Kamphuis, M. M. J.; Ferguson, C.; Parton, R. G.; Nice, E. C.; Heath, J. K.; Caruso, F. Uptake and Intracellular Fate of Disulfide-Bonded Polymer Hydrogel Capsules for Doxorubicin Delivery to Colorectal Cancer Cells. *ACS Nano* **2010**, *4*, 2928–2936.
39. Low, P. S.; Henne, W. A.; Doorneweerd, D. D. Discovery and Development of Folic-Acid-Based Receptor Targeting for Imaging and Therapy of Cancer and Inflammatory Diseases. *Acc. Chem. Res.* **2008**, *41*, 120–129.
40. Guo, X.; Shi, C.; Wang, J.; Di, S.; Zhou, S. B. pH-Triggered Intracellular Release from Actively Targeting Polymer Micelles. *Biomaterials* **2013**, *34*, 4544–4554.
41. Dai, J.; Lin, S. D.; Cheng, D.; Zou, S. Y.; Shuai, X. T. Interlayer-Crosslinked Micelle with Partially Hydrated Core Showing Reduction and pH Dual Sensitivity for Pinpointed Intracellular Drug Release. *Angew. Chem., Int. Ed. Engl.* **2011**, *50*, 9404–9408.
42. Li, M. Q.; Tang, Z. H.; Lv, S. X.; Song, W. T.; Hong, H.; Jing, X. B.; Zhang, Y. Y.; Chen, X. S. Cisplatin Crosslinked pH-Sensitive Nanoparticles for Efficient Delivery of Doxorubicin. *Biomaterials* **2014**, *35*, 3851–3864.
43. Lv, S. X.; Tang, Z. H.; Li, M. Q.; Lin, J.; Song, W. T.; Liu, H. Y.; Huang, Y. B.; Zhang, Y. Y.; Chen, X. S. Co-Delivery of Doxorubicin and Paclitaxel by PEG-Polypeptide Nanovehicle for the Treatment of Non-Small Cell Lung Cancer. *Biomaterials* **2014**, *35*, 6118–6129.
44. Thambi, T.; Deepagan, V. G.; Yoon, H. Y.; Han, H. S.; Kim, S. H.; Son, S.; Jo, D. G.; Ahn, C. H.; Suh, Y. D.; Kim, K.; *et al.*

Hypoxia-Responsive Polymeric Nanoparticles for Tumor-Targeted Drug Delivery. *Biomaterials* **2014**, *35*, 1735–1743.
45. Gabizon, A. A. Selective Tumor Localization and Improved Therapeutic Index of Anthracyclines Encapsulated in Long-Circulating Liposomes. *Cancer Res.* **1992**, *52*, 891–896.
46. Kataoka, K.; Matsumoto, T.; Yokoyama, M.; Okano, T.; Sakurai, Y.; Fukushima, S.; Okamoto, K.; Kwon, G. S. Doxorubicin-Loaded Poly(Ethylene Glycol)-Poly(Beta-Benzyl-L-Aspartate) Copolymer Micelles: their Pharmaceutical Characteristics and Biological Significance. *J. Controlled Release* **2000**, *64*, 143–153.
47. Lee, E. S.; Na, K.; Bae, Y. H. Doxorubicin Loaded pH-Sensitive Polymeric Micelles for Reversal of Resistant MCF-7 Tumor. *J. Controlled Release* **2005**, *103*, 405–418.
48. Al-Jamal, W. T.; Al-Ahmady, Z. S.; Kostarelos, K. Pharmacokinetics & Tissue Distribution of Temperature-Sensitive Liposomal Doxorubicin in Tumor-Bearing Mice Triggered with Mild Hyperthermia. *Biomaterials* **2012**, *33*, 4608–4617.
49. Xiao, J.; Duan, X.; Yin, Q.; Zhang, Z.; Yu, H.; Li, Y. Nanodiamonds-Mediated Doxorubicin Nuclear Delivery to Inhibit Lung Metastasis of Breast Cancer. *Biomaterials* **2013**, *34*, 9648–9656.
50. Maksimenko, A.; Dosio, F.; Mougin, J.; Ferrero, A.; Wack, S.; Reddy, L. H.; Weyn, A. A.; Lepeltier, E.; Bourgaux, C.; Stella, B.; *et al.* A Unique Squalenoylated and Nonpegylated Doxorubicin Nanomedicine with Systemic Long-Circulating Properties and Anticancer Activity. *Proc. Nat. Acad. Sci. U. S. A.* **2014**, *111*, E217–E226.
51. Ren, Y.; Wang, R. R.; Liu, Y.; Guo, H.; Zhou, X.; Yuan, X. B.; Liu, C. Y.; Tian, J. G.; Yin, H. F.; Wang, Y. S.; *et al.* A Hematoporphyrin-Based Delivery System for Drug Resistance Reversal and Tumor Ablation. *Biomaterials* **2014**, *35*, 2462–2470.
52. Smola, M.; Vandamme, T.; Sokolowski, A. Nanocarriers as Pulmonary Drug Delivery Systems to Treat and to Diagnose Respiratory and Non Respiratory Diseases. *Int. J. Nanomed.* **2008**, *3*, 1–19.
53. Maeda, H.; Wu, J.; Sawa, T.; Matsumura, Y.; Hori, K. Tumor Vascular Permeability and the EPR Effect in Macromolecular Therapeutics: a Review. *J. Controlled Release* **2000**, *65*, 271–284.
54. Fan, H.; Hu, Q. D.; Xu, F. J.; Liang, W. Q.; Tang, G. P.; Yang, W. T. *In Vivo* Treatment of Tumors Using Host-Guest Conjugated Nanoparticles Functionalized with Doxorubicin and Therapeutic Gene pTRAIL. *Biomaterials* **2012**, *33*, 1428–1436.
55. Wang, W. W.; Cheng, D.; Gong, F. M.; Miao, X. M.; Shuai, X. T. Design of Multifunctional Micelle for Tumor-targeted Intracellular Drug Release and Fluorescent Imaging. *Adv. Mater.* **2012**, *24*, 115–120.
56. Zhang, Z.; Qu, Q. Q.; Li, J. R.; Zhou, S. B. The Effect of the Hydrophilic/Hydrophobic Ratio of Polymeric Micelles on their Endocytosis Pathways into Cells. *Macromol. Biosci.* **2013**, *13*, 789–798.